



Journal of Geophysical Research: Oceans

RESEARCH ARTICLE

10.1002/2014JC010678

Kev Points:

- New Parameterization of basal stress associated with grounded ice keels
- Landfast ice area simulated is compared to observations
- The parameterization improves the simulation of Arctic coastal landfast ice

Correspondence to:

J.-F. Lemieux, jean-francois.lemieux@ec.gc.ca

Citation:

Lemieux, J.-F., L. B. Tremblay, F. Dupont, M. Plante, G. C. Smith, and D. Dumont (2015), A basal stress parameterization for modeling landfast ice, *J. Geophys. Res. Oceans*, *120*, 3157–3173, doi:10.1002/2014JC010678.

Received 23 DEC 2014
Accepted 30 MAR 2015
Accepted article online 3 APR 2015
Published online 28 APR 2015

A basal stress parameterization for modeling landfast ice

Jean-François Lemieux¹, L. Bruno Tremblay², Frédéric Dupont³, Mathieu Plante², Gregory C. Smith¹, and Dany Dumont⁴

¹Recherche en Prévision Numérique Environnementale/Environnement Canada, Dorval, Québec, Canada, ²Department of Atmospheric and Oceanic Sciences, McGill University, Montréal, Québec, Canada, ³Service Météorologique du Canada, Environnement Canada, Dorval, Québec, Canada, ⁴Institut des Sciences de la mer de Rimouski, Université du Québec à Rimouski, Rimouski, Québec, Canada

Abstract Current large-scale sea ice models represent very crudely or are unable to simulate the formation, maintenance and decay of coastal landfast ice. We present a simple landfast ice parameterization representing the effect of grounded ice keels. This parameterization is based on bathymetry data and the mean ice thickness in a grid cell. It is easy to implement and can be used for two-thickness and multithickness category models. Two free parameters are used to determine the critical thickness required for large ice keels to reach the bottom and to calculate the basal stress associated with the weight of the ridge above hydrostatic balance. A sensitivity study was conducted and demonstrates that the parameter associated with the critical thickness has the largest influence on the simulated landfast ice area. A 6 year (2001–2007) simulation with a 20 km resolution sea ice model was performed. The simulated landfast ice areas for regions off the coast of Siberia and for the Beaufort Sea were calculated and compared with data from the National Ice Center. With optimal parameters, the basal stress parameterization leads to a slightly shorter landfast ice season but overall provides a realistic seasonal cycle of the landfast ice area in the East Siberian, Laptev and Beaufort Seas. However, in the Kara Sea, where ice arches between islands are key to the stability of the landfast ice, the parameterization consistently leads to an underestimation of the landfast area.

1. Introduction

Landfast ice is sea ice that stays immobile or almost immobile near a coast over a certain time interval. It can be found in many coastal regions of the Arctic, typically forming in the fall and lasting until the next late-spring or early summer. In the Chukchi and Beaufort Seas, landfast ice starts to form in October–November. It becomes stable a few weeks later and it is maintained until May–June when it rapidly breaks up with the return of warmer temperatures [Mahoney et al., 2014]. In these regions, the landfast ice cover can extend a few tens of km away from the coast. Landfast ice is also found off the east coast of Greenland, in some coastal regions of Baffin Bay and in the Canadian Arctic Archipelago where land confinement helps to maintain a stable ice cover over many months. It is however off the coast of Siberia that landfast ice is the most prominent as it can extend hundreds of km into the sea [Reimnitz et al., 1994; Dethleff et al., 1998; Bareiss and Görgen, 2005]. Large areas of landfast ice are observed in the East Siberian, the Laptev and the Kara Seas [Yu et al., 2014].

Landfast ice affects the transfer of momentum between the atmosphere and the ocean, it often leads to a thinner coastal ice cover (as only thermodynamic growth occurs [Johnson et al., 2012; Itkin et al., 2015]), it determines the offshore position of polynyas [Dethleff et al., 1998], it can decouple winter river plumes from the atmosphere and it can affect the stability of the Arctic halocline [Itkin et al., 2015].

How landfast ice is formed and maintained is not fully understood yet but it is thought that the following mechanisms can play a role: restrictive geometry and the presence of islands [Divine et al., 2005], grounded ice keels acting as anchor points [Haas et al., 2005; Mahoney et al., 2007, 2014] and sea ice tensile strength [Tremblay and Hakakian, 2006]. Furthermore, it is recognized that landfast ice cover in different regions might be maintained by different mechanisms (or combination of mechanisms). Along the coast of Alaska, some studies clearly identify that grounded ice keels act as anchor points for the formation and

© 2015. The Authors.

This is an open access article under the terms of the Creative Commons Attribution-NonCommercial-NoDerivs License, which permits use and distribution in any medium, provided the original work is properly cited, the use is non-commercial and no modifications or adaptations are made.

maintenance of the landfast ice cover [Reimnitz et al., 1994; Mahoney et al., 2007, 2014]. In the Laptev Sea, some authors also point out that ice keels are involved in stabilizing the landfast ice cover [Haas et al., 2005]. Other studies, however, suggest that ice keels play a minor role [Reimnitz et al., 1994; Eicken et al., 2005] and that river water plumes instead are the primary drivers [Eicken et al., 2005]. In the Kara Sea, a series of archipelagos contribute to the stabilization of the landfast ice cover [Divine et al., 2005; Ólason, 2012]. The ice arch in Nares Strait can form because the sea ice cover can resist tensile stresses [Dumont et al., 2009].

Despite the importance of landfast ice for atmosphere-ice-ocean interactions, most large-scale sea ice models are either unable to simulate it or they represent it quite crudely. *Johnson et al.* [2012] used a mask to define regions where they set the ice velocity to zero between 1 November and 1 May of each year. They demonstrated the importance of landfast ice in limiting the ice growth due to dynamics. This approach does not lead to interannual variability. *Rozman et al.* [2011] used a similar approach by specifying monthly landfast ice masks derived from observations. *Lieser* [2004] set the ice velocity to zero when the ice thickness exceeded a certain thickness over a defined water depth. *Wang et al.* [2014] analyzed the landfast ice simulated by their ice-ocean model along the Alaskan coast. Grid cells assumed to be landfast were defined as those in water shallower than 35 m and with a velocity smaller than 4 cm s⁻¹ (i.e., a drift speed that is similar to the mean winter Arctic Ocean sea ice drift).

More sophisticated approaches were recently introduced. König Beatty and Holland [2010] have modeled landfast ice by adding isotropic tensile strength to a viscous-plastic sea ice model. They demonstrated, in 1-D experiments, that landfast ice can be stable over many weeks with this approach. Ólason [2012] was able to model landfast ice in the Kara Sea region by using a high resolution grid and by adjusting the sea ice mechanical parameters in a viscous-plastic sea ice model. Following the work of König Beatty and Holland [2010], Itkin et al. [2015] added isotropic tensile strength and increased the ice strength parameter in regions within the 30 m isobath. As the region where this parameterization is applied is fixed (within the 30 m isobath), it is questionable whether this approach can reproduce the interannual variability of landfast ice.

The main objective of this manuscript is to introduce a simple parameterization for large-scale sea ice models of the basal stress associated with grounded ice keels. Where the water depth is typically below 20–30 m, observations show that ice pressure keels can reach the bottom of the ocean and even penetrate the seabed and form gouges [Mahoney et al., 2007]. When these ridges are well grounded and offer sufficient support, they can act as anchor points and maintain the ice fast.

The model first calculates the critical mean ice thickness required for a large keel to reach the ocean floor. If the mean thickness is larger than the critical one, a new basal stress term, included in the momentum equation, mimics the ice anchoring on the ocean floor. This approach has some similarities with what was used by Lieser [2004] where the ice velocity was set to zero when the mean thickness reached a certain fraction of the water depth (therefore assuming that an ice keel is grounded). However, our approach is more physically based in the sense that an additional stress term is added to the momentum equation instead of prescribing a zero velocity when a keel touches the sea floor. Moreover, detachment events can be represented as the basal stress formulation involves a maximum stress that can be sustained by the keel. To our knowledge, our parameterization is the first attempt to represent the basal stress associated with grounded ice keels. This parameterization involves only a few free parameters. As it estimates the basal stress based on bathymetry data, ice concentration and the mean thickness in a grid cell, it can therefore be used for both two-thickness and multithickness category models.

Other objectives of this paper are to compare the simulated landfast ice cover to observations and to perform a sensitivity study to the basal stress free parameters; the goal is not to perform a thorough optimization of the free parameters.

This paper is structured as follows. Section 2 describes the sea ice momentum and continuity equations. The basal stress parameterization is described in section 3. A guide for the numerical implementation of the parameterization is provided in section 4. Some information about the sea ice model used in the experiments is given in section 5. An estimation of the free parameters associated with the parameterization is provided in section 6. The results of the numerical experiments are described in section 7. A discussion, concluding remarks and a description of future work are provided in section 8.

2. Sea Ice Momentum and Continuity Equations

Sea ice dynamics is often considered to be a two-dimensional problem [Coon et al., 1974]. This is justified by the large ratio between the horizontal and the vertical scales. The two-dimensional sea ice momentum equation is obtained by integrating in the vertical the momentum equation. It is given by

$$\rho_{i}h\frac{D\mathbf{u}}{Dt} = -\rho_{i}hf\mathbf{k} \times \mathbf{u} + \tau_{a} - \tau_{w} + \nabla \cdot \sigma - \rho_{i}hg\nabla H_{d}, \tag{1}$$

where ρ_i is the density of the ice, h is the ice volume per unit area (or the mean thickness), $\frac{D}{Dt}$ is the total derivative, f the Coriolis parameter, $\mathbf{u} = u\mathbf{i} + v\mathbf{j}$ the horizontal sea ice velocity vector, \mathbf{i} , \mathbf{j} and \mathbf{k} are unit vectors aligned with the x, y and z axis of our Cartesian coordinates, τ_a is the wind stress, τ_w the water stress, σ the internal ice stress tensor, g the gravity and H_d the sea surface height.

In our model, the advection of momentum is neglected. There is no snow cover. The sea surface tilt is expressed in terms of the geostrophic ocean current (as in *Tremblay and Mysak* [1997]). The stresses τ_a and τ_w are defined using a quadratic law with constant turning angles [*McPhee*, 1975]. The model is based on a viscous-plastic rheology with an elliptical yield curve [*Hibler*, 1979]. The ice strength is parameterized as $P = P^* h \exp^{-C(1-A)}$ where A is the ice concentration while P^* and C are constants [*Hibler*, 1979]. To avoid nonzero internal stresses when there is no forcing, a replacement closure similar to the one presented in *Kreyscher et al.* [2000] is used.

For a two-thickness category model, the continuity equations for the mean thickness and the concentration are given by

$$\frac{\partial h}{\partial t} + \nabla \cdot (\mathbf{u}h) = S_h, \tag{2}$$

$$\frac{\partial A}{\partial t} + \nabla \cdot (\mathbf{u}A) = S_A, \tag{3}$$

where S_h and S_A are thermodynamic source terms. Note that A is capped to 1.0. This does not affect the conservation of mass as the mass per m^2 is given by $\rho_i h$.

3. Basal Stress Parameterization

We develop a simple parameterization, for use in large-scale sea ice models, of the basal stress associated with subgrid scale grounded ice keels. The idea is to define a basal stress term $-\tau_b$ added to the right hand side of equation (1). The parameterization is based entirely on bathymetry data and prognostic variables from the model (h) the mean thickness in a grid cell and h0 the ice concentration). It could therefore be used for two-thickness category models (sometimes referred to as one-thickness category models, i.e., models that simulate the mean thickness in a grid cell and the ice concentration) as well as for multithickness category models. A more sophisticated approach would be to develop a parameterization based on the subgrid scale thickness distribution. Also, while the water depth is obtained solely here from bathymetry data, it would be better to take into account ocean surface elevation variations (due to tides, storm surge and ocean dynamics). These improvements are beyond the scope of this paper and the subject of future work.

Figure 1 is a cartoon that shows sea ice in shallow water. The ice field is viewed along the x axis. Δx corresponds to the size of the grid cell in the x direction. It is assumed that the ice conditions do not vary along the y axis. With Δy , the length of the grid cell in the other direction, the surface of the grid cell is $S = \Delta x \Delta y$. The length covered by ice along the x axis is I_i which means that the concentration A is given by $I_i \Delta y / \Delta x \Delta y = I_i / \Delta x$.

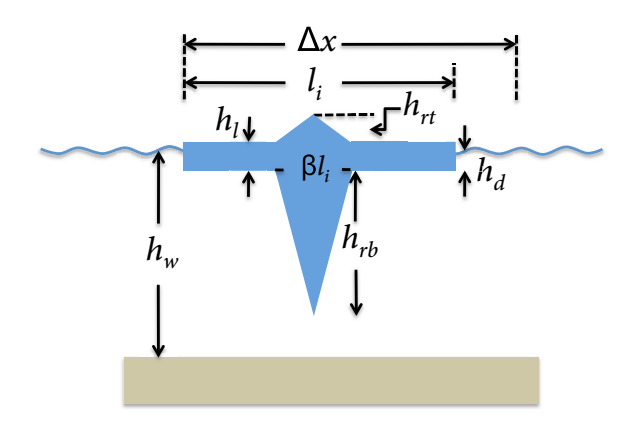


Figure 1. Cartoon showing sea ice in shallow water. The size of the grid cell is Δx along the x axis and Δy in the other direction. The length covered by ice along the x axis is I_i . The ice conditions do not vary along the y axis. The water depth is h_w . Most of the ice has a thickness of h_l . There is a ridge in the middle with a total thickness of $h_l + h_{rb} + h_{rt}$ with a surface at its base of $\beta l_l \Delta y$. The draft of the level ice is h_d .

ridge is considered to be triangular [Hibler, 1980]. The base of the ridge is assumed to be βl_i where $\beta \ll 1$. In fact, in our conceptual model, β should be viewed as the fraction of l_i covered by these large ridges (for clarity only one ridge is displayed in Figure 1). To simplify our formulation, β is considered to be a constant (which in reality is not). Reasonable values for β could be O(0.01).

We recall that we want to develop a parameterization that could be used for two-thickness category models. Hence, the model does not know h_t , h_{rb} and h_{rt} but only h the mean thickness in a grid cell and h the sea ice concentration.

Assuming hydrostatic balance and a constant ice density for the ridge and the level ice, we get the following equation for the level ice

$$\rho_i h_l = \rho_w h_d, \tag{4}$$

and the following equation for the ridge

$$\rho_{i}q\left[h_{l}+\frac{1}{2}(h_{rt}+h_{rb})\right]=\rho_{w}q(h_{d}+\frac{h_{rb}}{2}),$$
(5)

where h_d is the ice draft for the level ice and q=1-p. We kept q on both sides of equation (5) to show the dependance of the weight of the ridge and of the weight of the displaced water on the porosity. Based on the mass of ice in a grid cell, we can express h as

$$h = Ah_I(1 - \beta + \beta q) + A\beta q \left[\frac{h_{rt} + h_{rb}}{2} \right]. \tag{6}$$

Amundrud et al. [2004] and Melling and Riedel [1996] provide measurements of ice keels in the Arctic. From their measurements, one can obtain a relation between the total draft of large ice keels and the draft of the level ice. From Figure 1, the total draft of the ice keel is $h_{rb} + h_d$. Assuming a simple linear relationship, we get

$$h_{rb} + h_d = \gamma h_d, \tag{7}$$

where γ is a constant of proportionality. We notice from the data of *Amundrud et al.* [2004, Figure 5] that $\gamma = 10$ fits reasonably well the data. Note that our assumption that most of the grid cell is covered by level ice leads to an overestimation of the size of ice keels in regions of highly deformed ice.

Using equations (4–7), we can express h_l as a function of h as

$$h_l = \frac{2(h/A)}{(2-2\beta+\beta q+\beta q\gamma)}.$$
 (8)

We also find that h_{rt} and h_{rb} are respectively

$$h_{rt} = \frac{(\gamma - 1)(\rho_w - \rho_i)}{\rho_w} h_I, \tag{9}$$

$$h_{rb} = \frac{(\gamma - 1)\rho_i}{\rho_w} h_l. \tag{10}$$

We now have the dimensions of the ridge expressed in terms of h (and A). For a certain water depth h_{wr} the ice keel barely touches the seabed if the total draft is equal to $h_{rbc} + h_{dc}$ where the subscript c stands for

critical. The other ice thicknesses associated with h_{rbc} and h_{dc} are h_{lc} and h_{rtc} . As the ice barely touches the bottom, hydrostatic balance still holds and equations (4), (5), and (7) are valid (with h_l replaced by h_{lc} and so on for the other thicknesses).

For the critical thicknesses, we have

$$h_w = h_{rbc} + h_{dc} = \gamma h_{dc}. \tag{11}$$

Using equation (11), we can express the critical thickness of the level ice (in equation (4)) as a function of h_w . The relation is

$$h_{lc} = \frac{\rho_w h_w}{\gamma \rho_i} \,. \tag{12}$$

Using equation (8) with the critical mean thickness h_c and substituting it into equation (12) we get

$$\frac{h_c}{A} \left[\frac{2\rho_i \gamma}{\rho_w (2 - 2\beta + \beta q + \beta q \gamma)} \right] = h_w. \tag{13}$$

We define the term in front of h_c/A as k_1 , our first free parameter. This means that if k_1h/A is equal to h_{wr} the keel barely touches the seabed and h is the critical thickness h_c .

Let us assume that a large ridge, with vertical dimensions given by equations (8–10), was transported in shallower water by the winds and by ocean currents. For $h > h_c$, the keel is grounded at the bottom and hydrostatic balance does not hold anymore. In this case, there is a normal force pointing upward. We know that the normal force is zero for $h = h_c$. We determine here what is the normal force for $h > h_c$.

The ridge is now grounded where the water depth is h_w . The normal force is the weight of the ridge minus the weight of the displaced water. It is given by

$$F_{N} = \beta A Sg \rho_{i} q \left[h_{l} + \frac{h_{rt} + h_{rb}}{2} \right] - \beta A Sg \rho_{w} q \left[h'_{d} + \frac{h_{rb}}{2} \right]$$

$$\tag{14}$$

where h'_d is the nonhydrostatic draft. With $h'_d = h_w - h_{rb}$ and using equations (9) and (10), F_N is a much simpler expression as it becomes

$$F_N = \beta A Sgq(\rho_i \gamma h_l - \rho_w h_w). \tag{15}$$

Replacing h_w by k_1h_c/A and using equation (8), we get

$$F_{N} = \beta Sgq \left[\rho_{i} \gamma \frac{2h}{(2 - 2\beta + \beta q + \beta q \gamma)} - \rho_{w} k_{1} h_{c} \right]$$
(16)

Finally, using the definition of k_1 , one finds that

$$F_{N} = S \left[\frac{2\beta q \gamma \rho_{i} g}{(2 - 2\beta + \beta q + \beta q \gamma)} \right] (h - h_{c}), \tag{17}$$

i.e., the normal force is proportional to the difference between the mean thickness in the grid cell and the critical mean thickness h_c . Once the keel is grounded and h further increases (e.g., due to ridging events), equation (17) is still used to calculate the normal force. This can be done by assuming that the geometry of the grounded ridge is maintained (i.e., h_{rt} , h_l and h_{rb} increase but their ratios remain the same).

The basal stress parameterization presented here is based on the fact that the maximum friction force at the bottom is proportional to the normal force. When the landfast ice cover is stable, the friction force compensates for the forces due to the winds and ocean currents. Detachment of landfast ice does occur but the causes of these events remain unclear [Mahoney et al., 2007]. Mahoney et al. [2007] mention that air and ocean stresses might be insufficient and that other processes such as sea level surges or thermal erosion of keels might be at play when there is detachment event. Representing these processes is beyond the scope of this article.

Here we assume that the landfast cover can be stable for strong wind stress conditions but that very strong wind events could lead to a detachment of the landfast ice cover. When the wind blows relatively lightly,

the friction force compensates the wind force and the ice stays at rest. As the wind increases, the friction force could reach the maximum value

$$F_f = \mu_s F_N = \mu_s S \left[\frac{2\beta q \gamma \rho_i g}{(2 - 2\beta + \beta q + \beta q \gamma)} \right] (h - h_c), \tag{18}$$

where μ_s is the static friction coefficient. Note that the friction force needed to compensate the wind force depends on the fetch and the number of grid cells with anchor points (i.e., with an ice keel grounded at the seabed). We will get back to this point in section 6.

A gouging force [Mahoney et al., 2007] opposing the wind force might also exist but deriving an expression for this additional force is not an easy task and it is beyond the scope of this paper.

If the wind further increases, the ice could start to move. The friction force is then given by $F_f = \mu_k F_N$, where μ_k is the kinetic friction coefficient. Usually, μ_s is slightly larger than μ_k when two materials experience friction. Here we simply assume that $\mu_s = \mu_k = \mu$. Introducing $k_2 = \mu[2\beta q\gamma \rho_i g][2-2\beta+\beta q+\beta q\gamma]^{-1}$, F_f is given by $Sk_2(h-h_c)$. k_2 is our second free parameter (with units of Nm^{-3}).

For the implementation in our model, we divide F_f by the surface S and obtain a basal stress τ_b with units of Nm⁻². To represent the increase of the basal stress up to the maximal value $k_2(h-h_c)$ and to facilitate the implementation in our sea ice model we introduce the following formulation for the basal stress

$$\tau_{bu} = k_2 \left(\frac{u}{|\mathbf{u}| + u_0} \right) (h - h_c), \tag{19}$$

where τ_{bu} is the component of the basal stress aligned with the x axis (u component), $|\mathbf{u}| = \sqrt{u^2 + v^2}$ and u_0 is a small velocity parameter that allows one to define a smooth transition between the static and kinetic friction regimes. The same formulation is used for the v component.

In fact, in our formulation the ice is never completely at rest. For low wind stress, the ice is almost stopped and the basal stress is

$$\tau_{bu} \sim k_2 \frac{u}{u_0} (h - h_c), \tag{20}$$

and the 'residual' velocity decreases when using a smaller u_0 .

As the wind stress increases, the basal stress increases and it is limited by the maximum value

$$\tau_h^{\text{max}} = k_2(h - h_c). \tag{21}$$

We introduce one last modification to our basal stress parameterization. Large-scale sea ice models simulate the evolution of a thickness distribution (either the two-thickness category or the multithickness category models). When solving the momentum equation, one obtains at one grid point the same velocity for the entire thickness distribution. Assuming a loose pack with a few thick ridges, some keels could be grounded but overall the ice cover would not be landfast. The ice cover as a whole can be landfast only when the concentration is close to 1. Inspired by the ice strength formulation of [Hibler, 1979], we multiply the basal stress in equation (19) by a term that leads to a strong dependance of the basal stress on the sea ice concentration. With this term, our formulation of τ_b is given by

$$\tau_{bu} = \begin{cases} 0 & \text{if } h \le h_c, \\ k_2 \left(\frac{u}{|\mathbf{u}| + u_0} \right) (h - h_c) \exp^{-C_b(1 - A)} & \text{if } h > h_c, \end{cases}$$
 (22)

where $h_c = Ah_w/k_1$ and C_b is a constant set to 20 (as done in *Hibler* [1979] for the ice strength). Note that numerical simulations show that the exp ${}^{-C_b(1-A)}$ term has a small impact on the simulated landfast ice area (results not shown).

4. Numerical Implementation

The momentum equation is solved on a modified Arakawa C-grid (as shown in *Tremblay and Mysak* [1997, Figure 7a]). The bathymetry, h and A are defined at the tracer point (middle) with the u component on the left and v below. Here is how the basal stress is calculated for the u component in our model. A similar calculation is done for the v component.

To calculate τ_{bur} the basal stress for the u component, we need to know h_u , A_u , h_{wu} and v_u where the subscript u indicates that these quantities are defined at the u location. For u_{ij} , with i and j corresponding to the index of the grid cell, h_u is given by $\max\left[h_{i-1j},h_{ij}\right]$, A_u by $\max\left[A_{i-1j},A_{ij}\right]$, h_{wu} by $\min\left[h_{wi-1j},h_{wij}\right]$ and $|v_u|$ by $\min\left[|v_{i-1j}|,|v_{i-1j+1}|,|v_{ij+1}|,|v_{ij}|\right]$. Idealized numerical experiments (in 1-D and 2-D) have shown that the calculation of h_u as $\max\left[h_{i-1j},h_{ij}\right]$ instead of $\left[h_{i-1j}+h_{ij}\right]/2$ (same idea for A_u , h_{wu} and v_u) leads to a more stable and realistic landfast ice cover (results not shown).

In our model, the dynamics is solved with the implicit-explicit time integration scheme described in *Lemieux* et al. [2014] which is built around a Jacobian-free Newton-Krylov solver [*Lemieux* et al., 2010]. As h, A, and $\bf u$ evolve from one Newton iteration to the next, the max operation for calculating h_u (same idea for A_u and v_u) is expressed as

$$h_{u} = \frac{h_{i-1j} + h_{ij}}{2} + \frac{h_{i-1j}}{2} \tanh \left[\alpha (h_{i-1j} - h_{ij}) \right] + \frac{h_{ij}}{2} \tanh \left[\alpha (h_{ij} - h_{i-1j}) \right], \tag{23}$$

which provides a smooth transition due to the use of the hyperbolic tangents. The parameter α is set to 10^6 .

When the mean thickness h_u is lower than the critical value $h_{cu} = A_u h_{wu}/k_1$, the ice keel does not reach the bottom and the basal stress τ_{bu} is zero. However, if $h_u > h_{cu}$, the basal stress in the model is expressed as $\tau_{bu} = C_{bu} u$ with C_{bu} given by

$$C_{bu} = \left(\frac{k_2}{\sqrt{u^2 + v_u^2 + u_0}}\right) (h_u - h_{cu}) \exp^{-C(1 - A_u)}.$$
 (24)

This approach is easy to implement numerically as the basal stress term is similar to the water stress term. Note that to avoid calculating C_{bu} where there is little ice, this computation is done only if $A_u > 0.01$.

5. More Information About the Model

We use a relatively simple model to perform the simulations described in this paper. The sea ice model uses two thickness categories and a zero-layer thermodynamics. It is coupled thermodynamically to a slab ocean model. An upstream scheme is used for the advection operation of h and A. We use the latest model version described in *Lemieux et al.* [2014] with modifications for the landfast ice parameterization. The time integration scheme described in *Lemieux et al.* [2014] is used with operator splitting for the thermodynamic part. Details on thermodynamics are given in *Tremblay and Mysak* [1997].

The model domain covers the Arctic Ocean and the North Atlantic. Four spatial resolutions are available: 10, 20, 40 and 80 km (square cartesian grids). The simulations in this paper were done with a spatial resolution of 20 km. The land mask was created using the merged IBCAO/ETOPO5 bathymetry data of *Holland* [2000]. We use this data set for the water depth at each grid cell.

As opposed to what is usually done in the model, the mixed-layer depth of the slab ocean is not constant everywhere. For a specific grid cell, it is equal to the minimum value between the water depth at this location and 100 m. Due to the simplicity of this slab ocean model, the interpolated bathymetry on the 20 km grid is not allowed to be shallower than 5 m. The freezing point temperature is always assumed to be -1.8° C. The ocean currents are set to zero in the numerical experiments described here.

It is important to note that rheology parameters are set to the values used in most two-thickness category models [e.g., *Zhang and Hibler*, 1997; *Losch et al.*, 2010]. Hence, e = 2, $P^* = 27.5 \times 10^3$ N m⁻² and there is no isotropic tensile strength. These values were not modified in order to improve ice arching [*Dumont et al.*, 2009], a different landfast ice mechanism than the one investigated in this paper.

The wind stress is calculated using the geostrophic winds derived from the National Centers for Environmental Prediction and National Center for Atmospheric Research (NCEP/NCAR) 6 h reanalysis of sea level pressure [Kalnay et al., 1996]. Other atmospheric forcing fields also come from this reanalysis.

Table 1 lists the values of the physical parameters used for the simulations in this paper.

6. Estimation of Free Parameter Values

Our basal stress parameterization involves three free parameters. The parameter u_0 determines the small 'residual velocity' and provides a smooth transition between the basal stress in the static regime and the maximal basal stress. We have used $u_0 = 5 \times 10^{-5} \text{ ms}^{-1}$ in the experiments described below. The two important free parameters are k_1 and k_2 . A sensitivity study for k_1 and k_2 is performed in section 7.1. Here we estimate what could be typical values for these parameters.

As mentioned before, γ in equation (11) can be roughly estimated to 10 based on the data of *Amundrud* et al. [2004]. With A=1, $\gamma=10$ and p=1/3 (see Høyland [2002] for typical values of ridge porosity) in equation (13) we find that $k_1=8.54$ with $\beta=0.01$ while $k_1=7.74$ with a β five times larger. If we do the same thing for k_2 , assuming $\mu=0.5$, we find that it is equal to 286 Nm⁻³ with $\beta=0.01$ while it is equal to 1297 Nm⁻³ with a β five times larger. Notice that k_2 is very sensitive to the value of β .

The fact that the maximum basal stress increases with $h-h_c$ (i.e., the weight above hydrostatic balance) is realistic. However, we suspect that the maximum basal stress might be overestimated when estimating k_2 as described above. First, our derivation of the maximum basal stress does not take into account the characteristics of the seabed. A low density and porous seabed would not develop a large normal force (and therefore friction force). Second, the maximum basal stress could also be limited by zones of unconsolidated rubbles in the ice keel.

We therefore also consider the following approach to estimate k_2 . We assume that detachment events could occur for strong wind conditions. We consider a landfast ice cover 50 km long with a single anchor point at the edge. *Mahoney et al.* [2014] have shown the evidence of these anchor points off the coast of Alaska at distances on the order of a few tens of km. For the landfast ice to be stable, the basal force has to oppose the wind force (the integral of the wind stress over the 50 km long ice cover). We assume that the 50 km long ice cover is stable if the wind stress is smaller than 1 Nm⁻² (this corresponds to very strong wind conditions (\sim 25 ms⁻¹) as 0.1 Nm⁻² is a typical wind stress in the Arctic). With our parameterization, the basal stress is applied over the whole grid cell such that 50,000 $\tau_a = \Delta x \, \tau_b^{max} = \Delta x \, k_2 (h - h_c)$. With $\Delta x = 10$ km, we obtain

$$k_2 = \frac{5}{(h - h_c)},$$
 (25)

for the landfast ice to resist a wind stress of 1 Nm⁻².

Our estimate of k_2 depends on our estimate of $h-h_c$. As h is O(1 m), the largest values of $h-h_c$ are O(1 m) which leads to a lower bound estimate of $k_2 = 5 \text{ Nm}^{-3}$. With $h-h_c$ O(0.1 m) we find a k_2 10 times larger. Note that these estimates of k_1 and k_2 are used for guidance for our sensitivity study in section 7. Ultimately,

Table 1. Physical Parameters for the Numerical Simulations		
Symbol	Definition	Value
ρ_i	sea ice density	900 kg m ⁻³
ρ_a	air density	1.3 kg m^{-3}
$\rho_{\rm w}$	water density	1026 kg m^{-3}
C_{da}	air drag coefficient	1.2×10^{-3}
C_{dw}	water drag coefficient	5.5×10^{-3}
θ_{da}	air stress turning angle	25°
θ_{dw}	water stress turning angle	25°
f	Coriolis parameter	$1.46 \times 10^{-4} \text{s}^{-1}$
P*	ice strength parameter	$27.5 \times 10^{3} \text{ N m}^{-2}$
C	ice strength concentration	20
	parameter	
e	ellipse ratio	2

 k_1 and k_2 are tunable parameters that should be optimized through numerical experiments. In the light of the simple analysis described above, values of k_1 close to 10 and values of k_2 larger than 5 Nm⁻³ will be tested in our numerical simulations.

Our basal stress parameterization involves constant values of k_1 and k_2 in both space and time. This is an advantage as this leads to a simple approach that is easy to implement. However, the analysis above suggests that k_1 and

especially k_2 could vary significantly depending on the characteristics of the ridge and on the composition of the seabed. A more sophisticated approach would be to calculate the basal stress, at a certain location and for a specific time, based on the shape of the ridge, the surface in contact with the seabed, the shear strength of the unconsolidated part of the ridge and the composition of the seabed. This is beyond the scope of the present work.

7. Results

7.1. Sensitivity Study and Simulated Landfast Ice Area in the East Siberian, Laptev, Kara, and Beaufort Seas

In this section, we first present the results of a sensitivity study of the simulated landfast ice cover to the parameters k_1 and k_2 . A series of 6 year (September 2001 to September 2007) simulations are performed. A time step of 60 min is used. Initial conditions come from a long-term simulation with the standard model (i.e., without basal stress). The simulated LandFast (LF) ice area for the Laptev Sea is compared to the biweekly data from the *National Ice Center (NIC)* [2006].

The Laptev Sea was chosen for our sensitivity study for the following reasons. First, the NIC data reveal that, compared to the East Siberian, Kara, and Beaufort regions, it has a low interannual variability of LF area. Second, some authors [e.g., Haas et al., 2005] claim that grounded ice keels play a very important role in maintening the Laptev Sea LF ice cover (this is supported by our own analysis of MODIS images, not shown). Finally, the other regions have drawbacks for such a basal stress sensitivity study: ice arching is thought to be the dominant process for the Kara Sea LF ice cover, the LF ice along the Alaskan coast is very narrow and might not be well captured with our 20 km model and little is known about the mechanisms responsible for the East Siberian Sea LF ice cover.

We then investigate the simulated LF ice for three other regions that roughly correspond to the East-Siberian, the Kara and the Beaufort Seas. These regions are shown on our 20 km model grid in Figure 2. Similar regions were defined for the NIC data. As the data are on a 25 km resolution grid, the NIC land mask has differences with our 20 km land mask. Hence, the regions defined on the model 20 km mask are slightly different than the ones in the NIC data. Parts of the NIC water cells were eliminated to match our 20 km grid (e.g., our 20 km land mask does not include the Gulf of Ob). The difference in area between a region on the model grid and the equivalent NIC region is below 2% for the four regions. These regions are similar to the ones defined by *Yu et al.* [2014].

The bathymetry interpolated on our 20 km grid, for the Russian shelves and the Beaufort Sea are respectively shown in Figures 3 and 4. Extensive shallow shelves can be observed in Figure 3, especially in the East Siberian and Laptev Seas.

Figure 2. Model 20 km grid with regions used to calculate area of landfast ice. We refer to these as the East Siberian (in blue), the Laptev (in green), the Kara (in yellow) and the Beaufort (in red) regions. Land points are in gray.

The simulated biweekly LF area is calculated based on the mean magnitude of the velocity for each grid cell during the two week period. If for grid cell (i, j) the mean magnitude of the velocity is smaller than u_{crit} , Δx^2 is added to the LF area. Note that u_{crit} should be larger than the parameter u_0 . u_{crit} is set to 5×10^{-4} ms⁻¹ (which corresponds to a displacement of ~ 600 m during the two week period). The parameters for the basal stress parameterization sensitivity study are given in

Figure 5 displays the observed (in bold black) and simulated Laptev LF area for different values of the k_1

Table 2.

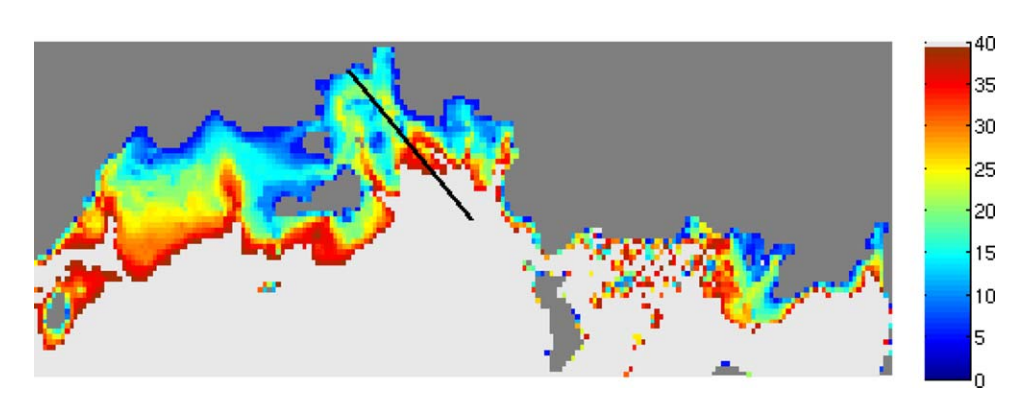


Figure 3. Water depth on a subdomain (Russian shelves) of the 20 km grid. The water depth is capped to 40 m to show the details on the Siberian shelves. The black line is a transect in the Laptev Sea that is used for one experiment.

and k_2 parameters. Also shown in Figure 5 is the simulated LF area by the standard model (i.e., without basal stress). The standard model usually does not have any LF ice but can on occasion simulate a certain LF ice cover due to the rheology term. These episodes often correspond to thick ice and low wind conditions (not shown). Overall, however, the standard model clearly underestimates the area of LF ice.

Between k_1 and k_2 , k_1 has the biggest impact. A larger k_1 parameter leads to higher LF area as well as a decreased monthly variability. For $k_1 = 6$, the area is underestimated (except for the winter of 2005/2006 which exhibit simulated thick ice conditions in the Laptev Sea, not shown). When doubling k_1 to 12, the area is always overestimated compared to the NIC data. It is found that $k_1 = 8$ provides a reasonable fit with the data.

With k_1 fixed to 8, the lower panel of Figure 5 shows that the simulated LF area varies only slightly for k_2 larger than 10 Nm⁻³; only $k_2 = 5$ Nm⁻³ leads to a notable difference. Note that while the results are insensi-

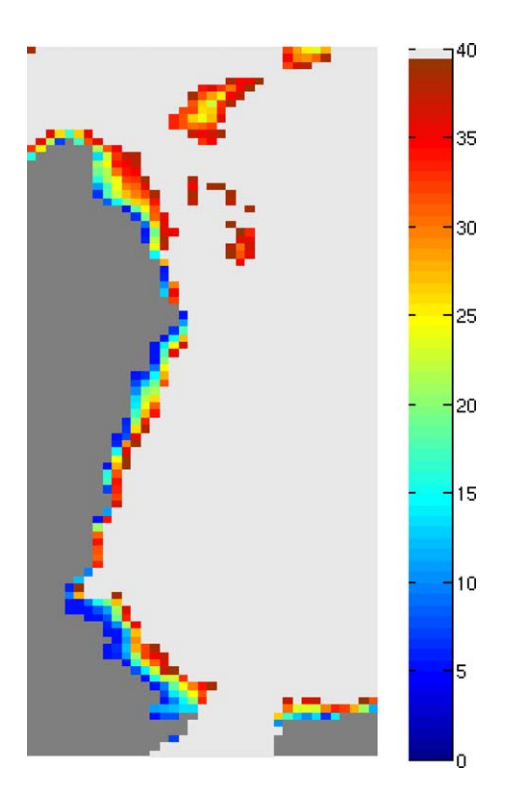
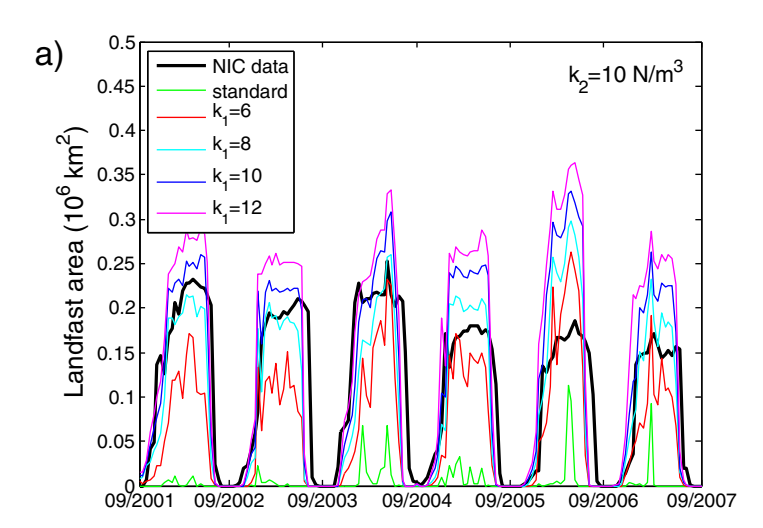


Figure 4. Water depth on a subdomain (Alaskan coast) of the 20 km grid. The water depth is capped to 40 m to show the details along the coast.

tive to k_2 for values larger than 10 Nm⁻³, this could be important in global warming simulations where the ice cover is thinner. The same conclusions about the effect of k_1 and k_2 on the simulated LF area can be drawn for the other regions (results not shown).

For the rest of the paper, all the results with the LF ice parameterization are for $k_1 = 8$ and $k_2 = 15 \text{ Nm}^{-3}$. Figure 6 shows the simulated LF area for the East Siberian (a), the Kara (b) and the Beaufort (c) regions. For the three regions, the standard model simulates very small areas of LF ice.

In the East Siberian Sea, an analysis of the observations in April (maximum extent) of each year for the period of interest (2002–2007) indicates that the LF ice cover roughly exhibit two modes: a small extent mode (2003, 2004, and 2007) with a concave U-shaped LF edge following the deeper tongue east of the New Siberian Islands (Novosibirkiye Ostrova) and a large mode (2002, 2005, and 2006) with the LF edge roughly



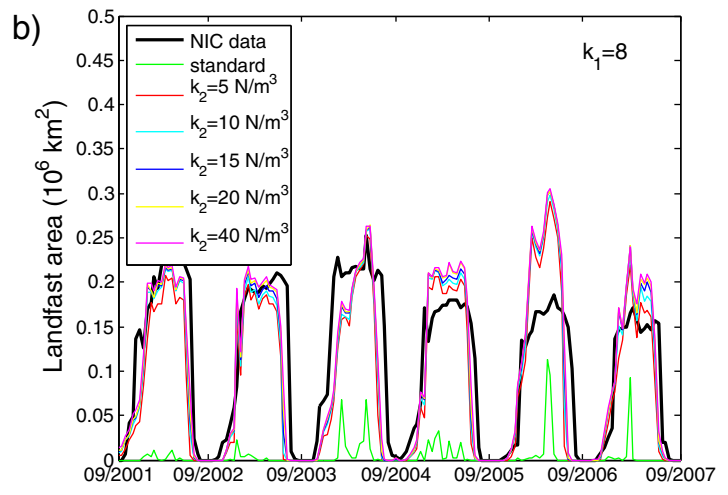


Figure 5. Area of landfast ice in the Laptev region as a function of time. The upper panel shows the sensitivity of the landfast area to the k_1 parameter (k_2 is fixed to $10 \, \mathrm{Nm}^{-3}$). The green curve is for the standard model and the red, cyan, blue, and magenta are respectively for $k_1 = 6$, 8, 10, and 12. The lower panel shows the sensitivity of the landfast area to the k_2 parameter (k_1 is fixed to 8). The green curve is for the standard model and the red, cyan, blue, yellow and magenta are respectively for $k_2 = 5$, 10, 15, 20, and 40 Nm $^{-3}$. In both panels, the bold black curve displays the area calculated from the NIC data.

following a straight line parallel to the north coast of the New Siberian Islands up to Siberian coast (results not shown). Interestingly, the model with $k_1 = 8$ and $k_2 = 15 \text{ Nm}^{-3}$ also has these two modes. It correctly simulates the small mode in 2003 and 2007 and the large mode in 2002, 2005, and 2006. However, in 2004, the large mode is simulated instead of the small one. Even though it simulates the mode, the model tends to overestimate the LF area. This is due to an overestimation of the LF cover north of the New Siberian islands. The simulated amplitude of the interannual variability is similar to the observed one (slightly larger for the model).

In the Kara region, there is consistently not enough LF simulated. The model performs quite well east of the Yamal peninsula but it simulates very little LF ice north of the Taymyr peninsula (southeastern part of the Kara region). This will be discussed later.

Considering the narrow band of LF observed off the coast of Alaska, the 20 km resolution model performs quite well in this region. The last year is especially well simulated: the maxi-

mum extent is right, the onset is a bit too late but the breakup happens at the same time than the observed one. The observations for the Beaufort region show a larger monthly variability than the simulated one.

Overall, it is found that the simulated LF season is shorter than observed in all regions. The timing of the simulated onset sometimes matches the observed onset but usually happens a few weeks later. The fact that the LF cover rapidly breaks up is well simulated by the model but it often happens a few weeks earlier (see e.g., Figure 5).

Table 2. Basal Stress Parameters for the Numerical Simulations			
Symbol	Definition	Value	
k ₁	critical thickness parameter	6, 8, 10, 12 5, 10, 15, 20, 40 N m ⁻³	
k ₂ C _b	maximum basal stress parameter basal stress ice concentration	5, 10, 15, 20, 40 N m ⁻²	
	parameter	F.v.10=5=1	
u ₀ u _{crit}	basal stress velocity parameter velocity criterion for landfast ice	$5 \times 10^{-5} \text{ ms}^{-1}$ $5 \times 10^{-4} \text{ ms}^{-1}$	

7.2. Transect in the Laptev Sea

To illustrate how the basal stress parameterization stabilizes the simulated ice cover, Figure 7 displays the values of the basal stress for the v component (a), the v component of velocity (b), the ice thickness (c) and the concentration

09/2001

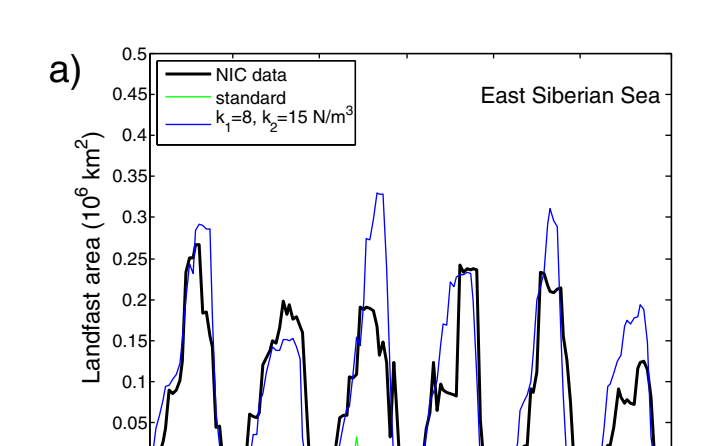
09/2002

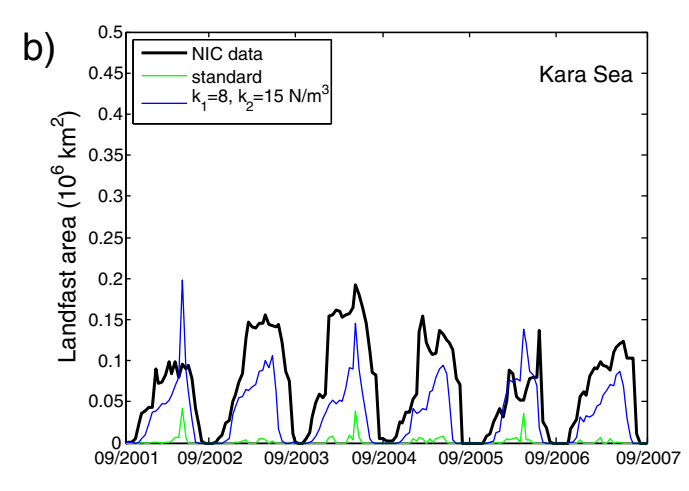
09/2003

09/2004

09/2005

09/2006





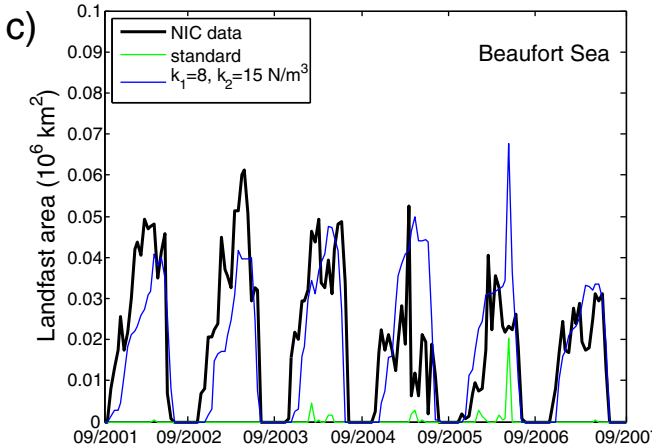


Figure 6. Area of landfast ice in the (a) East Siberian region, (b) the Kara region, and (c) the Beaufort region as a function of time. The green curves are for the standard model while the blue ones are for $k_1 = 8$ and $k_2 = 15 \text{ Nm}^{-3}$. In the three figures, the bold black curve displays the area calculated from the NIC data. Note that the scale is different in Figure 6c.

(d) along a \sim 800 km transect in the Laptev Sea (see Figure 3). Similar conclusions can be drawn with the basal stress u component and u component of velocity. The top of each panel coincides with the coast and the bottom to the most offshore grid point of the transect. Note that to better visualize the LF season in Figure 7b, the v component of velocity is displayed even when there is very little ice or no ice at all (free drift velocity). For clarity, only 1 year (10 September 2002 to 10 September 2003) of the simulation is presented.

Figure 7a indicates that three anchor regions are found along this transect. The ice first reaches the bottom at the coast. Later during the growth season, a second strong anchor region forms \sim 350 km from the coast. A less significant anchor point is seen in the middle of the LF cover at the end of the growth season. The offshore anchor region clearly gets thicker (and therefore stronger) due to ridging events (Figure 7c). Partial detachment events can be seen at the beginning or at the end of the season. However, once the growing season is sufficiently advanced (January), the LF cover is stable and the velocity is $\sim 0 \text{ ms}^{-1}$ from the coast up to the polynya. Compared to the standard model which simulates a polynya at the coast (not shown), the model with the basal stress parameterization exhibits a polynya ∼350 km from the coast at the landfast ice edge (Figures 7c and 7d).

7.3. Comparison Between the Standard Model and the Model With the Basal Stress Parameterization

An example is given here for evaluating the effect of the basal stress parameterization on the pan-Arctic

scale. Figures 8a, 9a, and 10a respectively show the simulated April 2002 monthly mean ice concentration, thickness and velocity for the standard model. These figures suggest that the simulated LF area is small. The ice velocity is non zero almost everywhere on the Siberian shelves. Moreover, there is evidence of coastal polynyas but no offshore polynyas (Figures 8a and 9a).

AGU Journal of Geophysical Research: Oceans

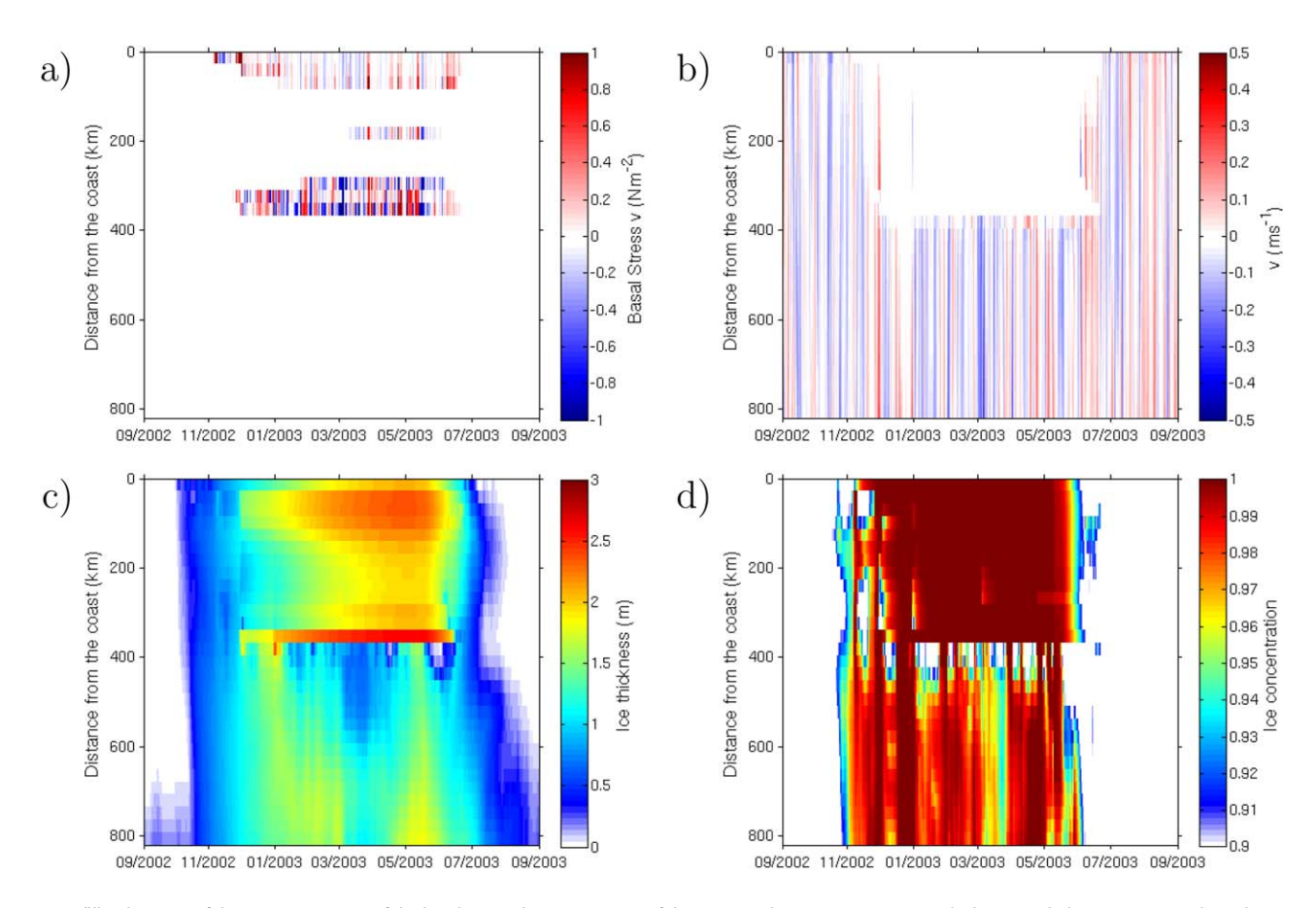


Figure 7. Hovmöller diagrams of the (a) v component of the basal stress, (b) v component of the sea ice velocity, (c) mean sea ice thickness, and (d) concentration along the transect shown in Figure 3. The y axis shows the distance from the coast along the transect while the x axis represents the dates for the period 10 September 2002 to 10 September 2003. The basal stress parameters are $k_1 = 8$ and $k_2 = 15$ Nm⁻³. For the four panels, the values are limited below (above) by the minimum (maximum) value of the colorbar (note that A is limited below to 0.9).

Figures 8b, 9b, and 10b respectively show the simulated April 2002 monthly mean concentration, thickness and ice velocity for the model with the LF parameterization. Compared to the standard model velocity field (Figure 10a), the simulated velocity field with the LF parameterization (Figure 10b) is near zero over large areas of the Laptev and East Siberian Seas. Impacts of the parameterization are also observed along the East coast of Greenland, close to Alaska and in the Kara Sea. A is very close to 1.0 in the regions with LF (as there is no deformation). Compared to the results with the standard model, the basal stress parameterization moves the coastal polynyas to offshore positions (mostly obvious in the East Siberian and Laptev Seas, see Figures 8b and 9b). Because of land confinement, both the standard simulation and the one with the basal stress parameterization exhibit LF ice in the Canadian Arctic Archipelago (Figures 10a and 10b).

8. Discussion and Concluding Remarks

We have introduced a simple LandFast (LF) ice parameterization for large-scale sea ice models. The parameterization calculates a critical mean sea ice thickness. When the simulated mean thickness is equal or larger than this critical thickness, the parameterization assumes that an ice keel is grounded. The maximum basal stress that can support the ice cover at this location then depends on the weight of the ridge above hydrostatic balance. This parameterization involves just a few free parameters, it is easy to implement and can be used for both two-thickness and multithickness category models. It leads to interannual variability of the simulated landfast area and of the timing of onset and breakup of the landfast ice cover.

To investigate this new parameterization, numerical experiments were performed with a two-thickness category sea ice model coupled to a slab ocean model. The simulated areas of LF ice were calculated for four



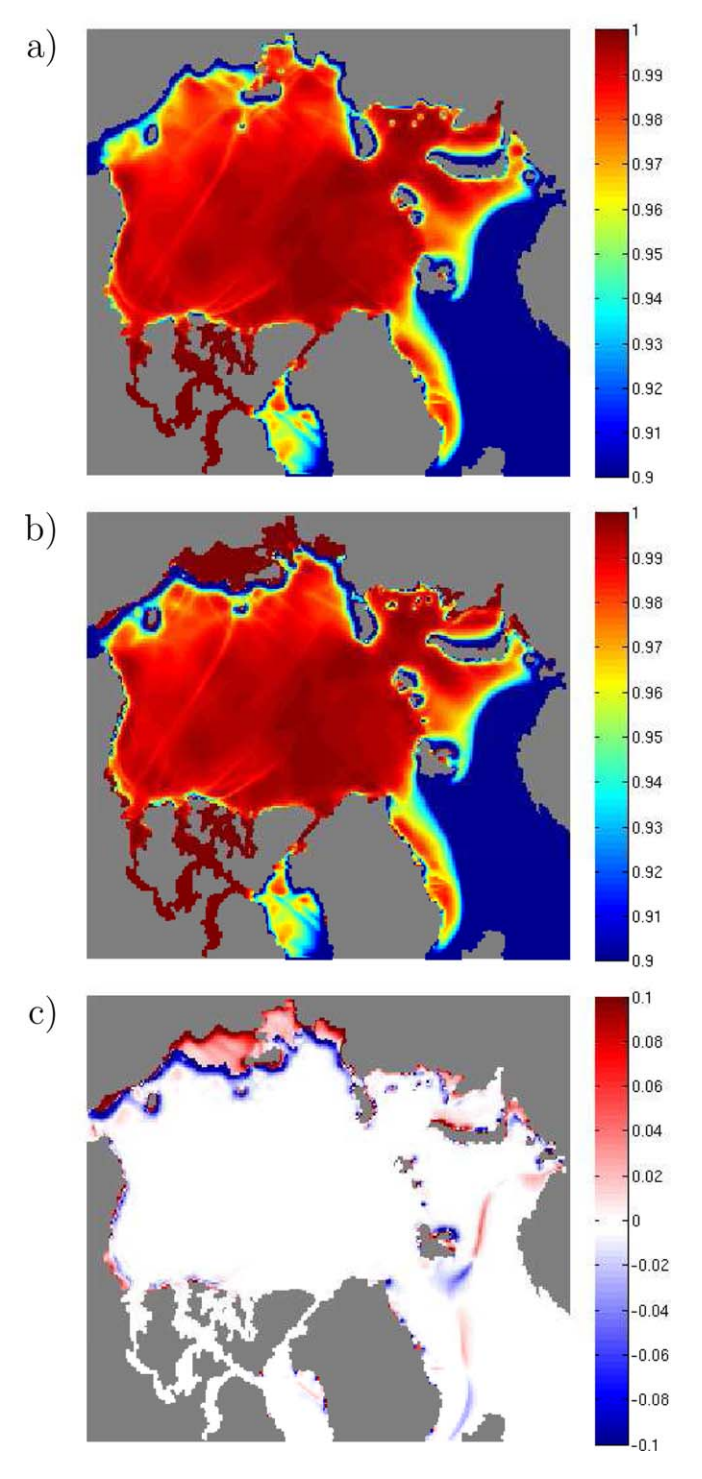


Figure 8. Monthly mean sea ice concentration field in April 2002 for the (a) standard model and (b) model with $k_1 = 8$ and $k_2 = 15$ Nm⁻³. Note that A is limited below to 0.9. (c) Difference between the monthly mean concentration field in April 2002 obtained with $k_1=8$ and $k_2=15~{\rm Nm}^{-3}$ and the one obtained with the standard model. The difference is limited below to -0.1 and capped to 0.1.

regions (roughly the Alaskan Coast, the East Siberian, the Laptev and the Kara Seas) and were compared to data from the National Ice Center [2006].

Compared to the standard model (without basal stress), the model with the basal stress parameterization leads to more realistic simulations. The standard model usually exhibit coastal polynyas while the one with the parameterization often positions the polynyas offshore as it is seen in the observations (e.g., in the Laptev Sea [Reimnitz et al., 1994]).

The model with the parameterization leads to a good simulation of the Laptev Sea LF area. As in the observations, the simulated maximum LF area has a small interannual variability. The model, however, tends to lead to an earlier breakup than what is seen in the observation (\sim 4 weeks). In the East Siberian Sea, as in the observations, the simulations roughly exhibit two modes of LF extent: a small mode with a concave offshore LF edge and a large mode with a straight offshore edge. The model, however, tends to overestimate the LF area in the East Siberian Sea. In the Kara Sea, the simulated LF area is clearly lower than what is seen in the observations and the LF season is shorter. Compared to the East Siberian and Laptev Seas, shallow shelves and high shoals are less present in the Kara Sea (especially in the Eastern Kara Sea). This suggests that our parameterization alone cannot simulate adequately the LF cover in the Kara Sea. Various parameterizations are probably necessary in largescale sea ice models to correctly simulate the LF ice cover. Modifications to our yield curve (ellipse ratio) [Dumont et al., 2009] as well as addition of isotropic tensile strength [König Beatty and Holland, 2010] are also probably required for simulating other mechanisms such as ice arching. Moreover, with a finer grid, additional small

islands would be present in the land mask and would probably foster the simulation of LF ice in the Kara Sea [Divine et al., 2005]. In the Beaufort Sea, the model with the basal stress parameterization performed quite well even though it was run at a relatively low spatial resolution (20 km).

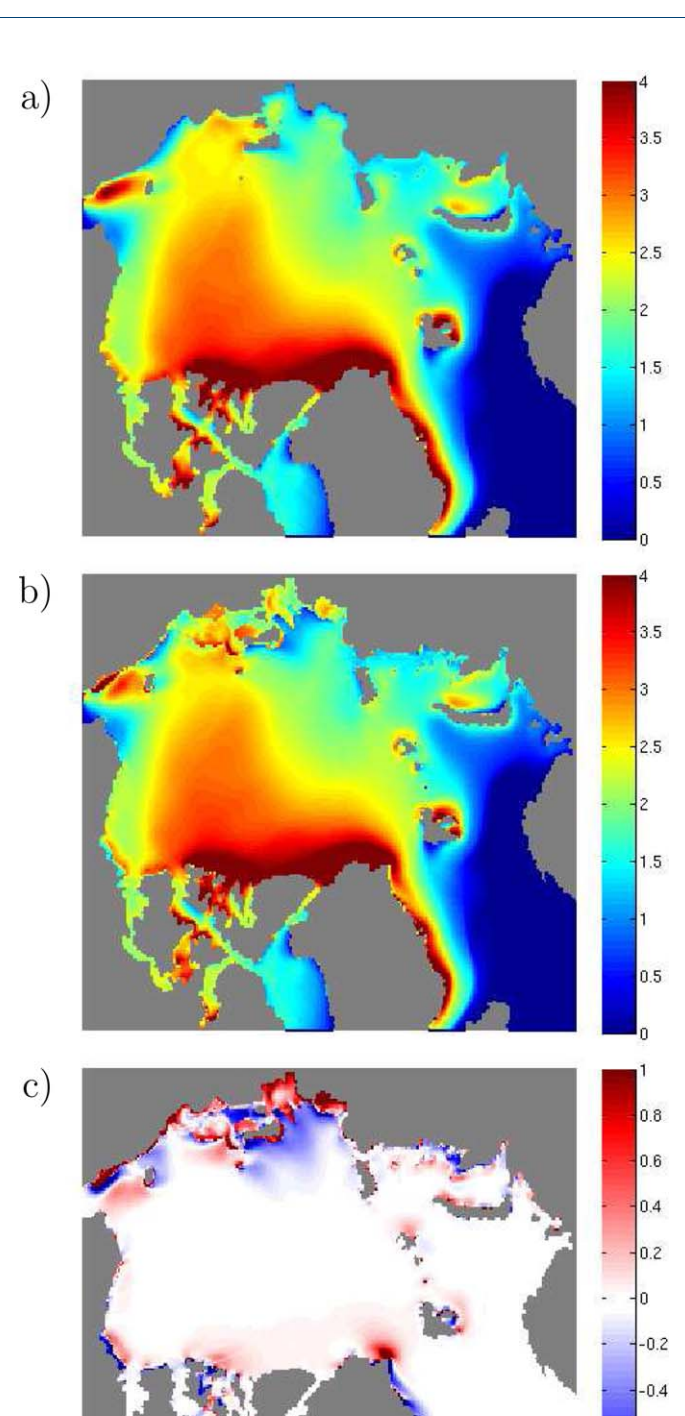


Figure 9. Monthly mean sea ice thickness field in April 2002 for the (a) standard model and (b) model with $k_1=8$ and $k_2=15~{\rm Nm}^{-3}$. (c) Difference between the monthly mean thickness field in April 2002 obtained with $k_1=8$ and $k_2=15~{\rm Nm}^{-3}$ and the one obtained with the standard model. The difference is limited below to $-1~{\rm m}$ and capped to $1~{\rm m}$.

Despite some success in simulating the LF cover, our basal stress parameterization has some limitations and weaknesses. We suspect the grounding process to be overrepresented compared to what happens in reality. As the growth season advances, the simulated LF ice cover gets stronger. It is often solidified as offshore anchor points get stronger due to multiple ridging events. Ridging events can also occur inside the LF region at the beginning of the season and consolidate/create anchor points. This is realistic. Anchor points are also solidified by thermodynamic growth which mimics the consolidation of ice keels. However, in reality, once the ice keel is fully consolidated (i.e., the porosity equals zero), our model will continue to add mass to the parameterized keel. This is unrealistic. Furthermore, once the ice is LF, the ice between anchor points continues to grow thermodynamically. If the mean thickness then reaches the critical thickness, the parameterization leads to a new ice keel that reaches the bottom. This creates an additional anchor point. This is unrealistic. This could be improved by preventing grid points for which the ice is already at rest to create additional anchor points. Another approach would be to use a multithickness category model to determine if an ice keel touches the sea floor. Explicitly representing 20-30 m ice keels in a multithickness category model is probably too computationally expensive for most applications. Hence, it might still be required to parameterize the grounding of ice keels based on a crude ice thickness distribution.

Compared to observations, the simulated LF season is usually shorter. As an example, in the Laptev Sea, the onset of LF ice is well simulated but the breakup systematically occurs a few weeks too early. As in the observations, however, the model with the

basal stress parameterization simulates a very rapid breakup of the LF ice cover. The premature LF breakup might be due to the fact that ice keels in the parameterization depend on the mean thickness. We suspect that our parameterized ice keels melt too quickly compared to real grounded ice keels as their melt

-0.6

-0.8

AGU Journal of Geophysical Research: Oceans

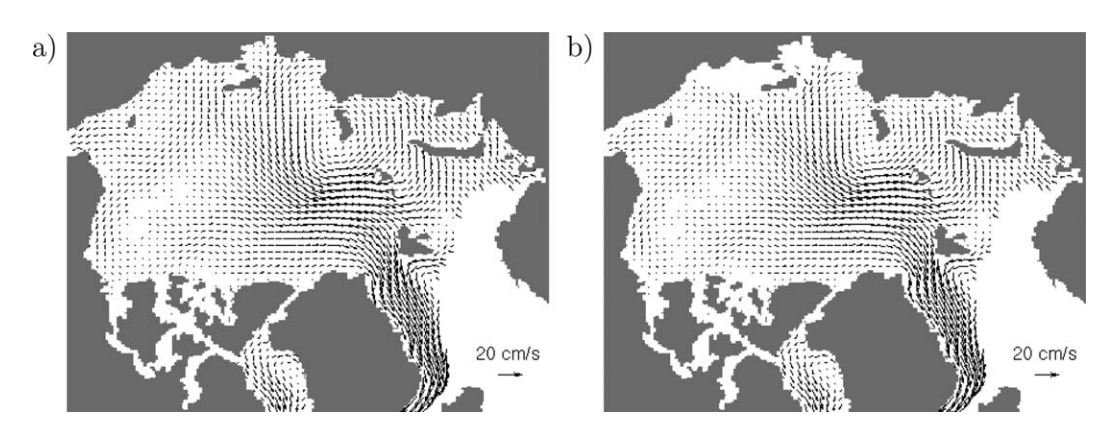


Figure 10. (a) Monthly mean sea ice velocity field in April 2002 for the standard model. (b) Monthly mean sea ice velocity field in April 2002 obtained with $k_1 = 8$ and $k_2 = 15$ Nm⁻³. For clarity, only one out of 16 velocity vectors is shown.

depends basically on the decrease of the mean thickness. Finally, the simulation of LF ice could be improved by correctly representing the influence of large river outflow on the coastal salinity. As our model does not take into account the effect of large rivers on the coastal salinity (the model assumes that the freezing point temperature is constant (-1.8°C) in space and time), it probably underestimates the initial growth of ice along the coast (which could help the initial development of LF ice). Tides, storm surge, keel consolidation and erosion, gouging force and sea floor composition are other processes that should also be taken into account for improving the simulation of LF ice.

Improving the representation of the anchor points and the timing of the LF onset and breakup is the subject of future work. To do so, we plan to test and improve our basal stress parameterization at higher resolution and with a more sophisticated model. This will be done with a recently developed $1/12^{\circ}$ coupled iceocean model which is based on the NEMO ocean model and the multithickness category CICE sea ice model.

Acknowledgments

We would like to thank Elizabeth Hunke and Andy Mahoney for their very helpful comments. We also want to thank Sylvain Bouillon for pointing out a mistake in the basal stress parameterization in an earlier version of this manuscript. The merged IBCAO/ ETOPO5 bathymetry data are available at efdl.cims.nyu.edu/project aomip/ forcing_data/topography/merged/ overview.html. The NCEP/NCAR 6 h reanalysis data can be found at www. esrl.noaa.gov/psd/data/gridded/data. ncep.reanalysis.html. The National Ice Center landfast ice data are available at http://nsidc.org/data/docs/noaa/ g02172_nic_charts_climo_grid/.

References

Amundrud, T. L., H. Melling, and R. G. Ingram (2004), Geometrical constraints on the evolution of ridged sea ice, J. Geophys. Res., 109, C06005, doi:10.1029/2003JC002251.

Bareiss, J., and K. Görgen (2005), Spatial and temporal variability of sea ice in the Laptev Sea: Analyses and review of satellite passivemicrowave data and model results, 1979 to 2002, Global Planet. Change, 48, 28-54, doi:10.1016/j.gloplacha.2004.12.004.

Coon, M. D., G. A. Maykut, R. S. Pritchard, D. A. Rothrock, and A. S. Thorndike (1974), Modeling the pack ice as an elastic-plastic material, AIDJEX Bull., 24, 1-105.

Dethleff, D., P. Loewe, and E. Kleine (1998), The Laptev Sea flaw lead-detailed investigation on ice formation and export during 1991/1992 winter season, Cold Rea. Sci. Technol., 27, 225-243.

Divine, D. V., R. Korsnes, A. P. Makshtas, F. Godtliebsen, and H. Svendsen (2005), Atmospheric-driven state transfer of shore-fast ice in the northeastern Kara Sea, J. Geophys. Res., 110, C09013, doi:10.1029/2004JC002706.

Dumont, D., Y. Gratton, and T. E. Arbetter (2009), Modeling the dynamics of the North water polynya ice bridge, J. Phys. Oceanogr., 39, 1448-1461, doi:10.1175/2008JPO3965.1.

Eicken, H., I. Dmitrenko, K. Tyshko, A. Darovskikh, W. Dierking, U. Blahak, J. Groves, and H. Kassens (2005), Zonation of the Laptev Sea landfast ice cover and its importance in a frozen estuary, Global Planet. Change, 48, 55-83, doi:10.1016/j.gloplacha.2004.12.005.

Haas, C., W. Dierking, T. Busche, and J. Hoelemann (2005), ENVISAT ASAR monitoring of polynya processes and sea ice production in the Laptev Sea, Proc. of the 2004 Envisat & ERS Symposium, Salzburg, Austria 6–10 September 2004.

Hibler, W. D. (1979), A dynamic thermodynamic sea ice model, J. Phys. Oceanogr., 9, 815–846.

Hibler, W. D. (1980), Modeling a variable thickness sea ice cover, Mon. Weather Rev., 108, 1943–1973.

Holland, D. M. (2000), Merged IBCAO/ETOPO5 Global Topographic Data Product, Natl. Geophys. Data Cent., Boulder, Colo.

Høyland, K. V. (2002), Consolidation of first-year sea ice ridges, J. Geophys. Res., 107(C6), 3062, doi:10.1029/2000JC000526.

Itkin, P., M. Losch, and R. Gerdes (2015), Landfast ice affects the stability of the Arctic halocline: Evidence from a numerical model, J. Geophys. Res. Oceans, doi:10.1002/2014JC010353, in press.

Johnson, M., et al. (2012), Evaluation of Arctic sea ice thickness simulated by Arctic Ocean Model Intercomparion Project models, J. Geophys. Res., 117, C00D13, doi:10.1029/2011JC007257.

Kalnay, E., et al. (1996), The NCEP/NCAR 40-year reanalysis project, Bull. Am. Meteorol. Soc., 77(3), 437–471.

König Beatty, C., and D. M. Holland (2010), Modeling landfast sea ice by adding tensile strength, J. Phys. Oceanogr., 40, 185–198, doi: 10.1175/2009JPO4105.1.

Kreyscher, M., M. Harder, P. Lemke, and G. M. Flato (2000), Results of the Sea Ice Model Intercomparison Project: Evaluation of sea ice rheology schemes for use in climate simulations, J. Geophys. Res., 105(C5), 11,299-11,320.

Lemieux, J.-F., B. Tremblay, J. Sedláček, P. Tupper, S. Thomas, D. Huard, and J.-P. Auclair (2010), Improving the numerical convergence of viscousplastic sea ice models with the Jacobian-free Newton Krylov method, J. Comput. Phys., 229, 2840-2852, doi:10.1016/j.jcp.2009.12.011.

- Lemieux, J.-F., D. A. Knoll, M. Losch, and C. Girard (2014), A second-order accurate in time IMplicit-EXplicit (IMEX) integration scheme for sea ice dynamics, J. Comput. Phys., 263, 375–392, doi:10.1016/j.jcp.2014.01.010.
- Lieser, J. L. (2004), A numerical model for short-term sea ice forecasting in the Arctic, PhD thesis, Universitat Bremen, Bremen, Germany. Losch, M., D. Menemenlis, J.-M. Campin, P. Heimbach, and C. Hill (2010), On the formulation of sea-ice models. Part 1: Effects of different solver implementations and parameterizations, *Ocean Modell.*, 33, 129–144, doi:10.1016/j.ocemod.2009.12.008.
- Mahoney, A., H. Eicken, and L. Shapiro (2007), How fast is landfast sea ice? A study of the attachment and detachment of nearshore ice at Barrow, Alaska, *Cold Reg. Sci. Technol.*, 47, 233–255, doi:10.1016/j.coldregions.2006.09.005.
- Mahoney, A. R., H. Eicken, A. G. Gaylord, and R. Gens (2014), Landfast sea ice extent in the Chukchi and Beaufort Seas: The annual cycle and decadal variability, *Cold Reg. Sci. Technol.*, 103, 41–56, doi:10.1016/j.coldregions.2014.03.003.
- McPhee, M. (1975), Ice-ocean momentum transfer for the AIDJEX ice model, AIDJEX Bull., 29, 93–111.
- Melling, H., and D. A. Riedel (1996), Development of seasonal pack ice in the Beaufort Sea during the winter of 1991–1992: A view from below, *J. Geophys. Res.*, 101(C5), 11,975–11,991.
- National Ice Center (2006), National Ice Center Arctic Sea Ice Charts and Climatologies in Gridded Format, edited and compiled by F. Fetterer and C. Fowley, Natl. Snow and Ice Data Cent., Boulder, Colo., doi:10.7265/N5X34VDB. [Available at http://nsidc.org/data/g02172/.]
- Ólason, E. Ö. (2012), Dynamical modeling of Kara Sea land-fast ice, PhD thesis, Univ. of Hamburg, Hamburg, Germany.
- Reimnitz, E., D. Dethleff, and D. Nürnberg (1994), Contrasts in Arctic shelf sea-ice regimes and some implications: Beaufort Sea versus Laptev Sea, Mar. Geol., 119, 215–225.
- Rozman, P., J. A. Hölemann, T. Krumpen, R. Gerdes, C. Köberle, T. Lavergne, S. Adams, and F. Girard-Ardhuin (2011), Validating satellite derived and modelled sea-ice drift in the Laptev Sea with in situ measurements from the winter of 2007/08, *Polar Res.*, 30, 7218, doi: 10.3402/polar.v30i0.7218.
- Timco, G. W., and R. P. Burden (1997), An analysis of the shapes of sea ice ridges, Cold Reg. Sci. Technol., 25, 65–77.
- Tremblay, B., and M. Hakakian (2006), Estimating the sea ice compressive strength from satellite-derived sea ice drift and NCEP reanalysis data, *J. Phys. Oceanogr.*, 36, 2165–2172.
- Tremblay, B., and L. A. Mysak (1997), Modeling sea ice as a granular material, including the dilatancy effect, *J. Phys. Oceanogr.*, 27, 2342–2360.
- Wang, J., K. Mizobata, X. Bai, H. Hu, M. Jin, Y. Yu, M. Ikeda, W. Johnson, W. Perie, and A. Fujisaki (2014), A modeling study of coastal circulation and landfast ice in the nearshore Beaufort and Chukchi seas using CIOM, J. Geophys. Res. Oceans, 119, 3285–3312, doi:10.1002/2013.IC009258.
- Yu, Y., H. Stern, C. Fowler, F. Fetterer, and J. Maslanik (2014), Interannual variability of Arctic landfast ice between 1976 and 2007, J. Clim., 27, 227–243. doi:10.1175/JCLI-D-13-00178.1.
- Zhang, J., and W. D. Hibler (1997), On an efficient numerical method for modeling sea ice dynamics, J. Geophys. Res., 102(C4), 8691–8702.